IEEE Access
Multidisciplinary | Rapid Review | Open Access Journal

Received April 16, 2019, accepted May 22, 2019, date of publication June 5, 2019, date of current version July 17, 2019.

Digital Object Identifier 10.1109/ACCESS.2019.2920968

Electric-Field Distribution and Insulation Status of ±800kV UHVDC Converter Valve After Implanting Full-View Micro-Sensor Detector

CHENYANG LIU[1,2], SIQUAN HU[1], KUN HAN[1], QIULING HU[1], SHILONG GAO[1], AND WEIZHENG YAO[1]

[1]State Grid Xuji Group Corporation, Xuchang 461000, China
[2]State Key Laboratory of Electrical Insulation and Power Equipment, Xi'an Jiaotong University, Xi'an 710049, China

Corresponding author: Chenyang Liu (liucheyan@126.com)

This work was supported in part by the State Grid Science and Technology Project under Grant 5200-201956058A-0-0-00, and in part by the Henan Postdoctoral Science Project (Research on EMI mechanism and protection technology of high potential circuit boards for VSC-HVDC converter).

ABSTRACT This paper explores how the installation of the full-view micro-sensor detector will affect the electric-field distribution of ±800-kV converter valve. We build the 3D model of ±800-kV converter valve tower and use Ansoft Maxwell 3D Field Simulator to study the electric-field distribution of ±800-kV converter valve tower with the full-view micro-sensor detector at different logical suitable locations. The results show that the installed locations have nearly no influence on the maximum electric-field distribution of non-direct contacted components; but for the direct-contacted components, the maximum electric-field has increased to a certain degree. The results further show that the electric-fields distribution especially the maximum electric-fields distribution at different locations is different, but the maximum electric-field value is still less than the 3 kV/mm. Thus, it can be concluded that the installation of full-view micro-sensor detectors can lead to an increase of maximum electric-field, but it has no influence on the insulation condition of valve tower, and the insulation design still meets the requirements well. Finally, the experiment validates that the installation of the full-view micro-sensor detector is feasible.

INDEX TERMS Full-view micro-sensor detector, ±800kV converter valve, valve component, electric-field simulation, maximum electric-field, insulation status.

I. INTRODUCTION

From the past few decades, electricity demand density is increasing in China, which urges utility companies to build transmission lines with a higher capacity to catch up with the increasing electricity demand efficiently. HVDC transmission lines have a high capacity to transmit electrical power with low power losses and other suitable sustainable transmission properties. Therefore, planning and implementation of HVDC systems are hot research topic nowadays [1]. The converter valve works as the vital equipment of the converter station of HVDC systems. It's proper working to ensure that the whole power grid can run safely and consistently. The converter valve tower can be divided into two categories; double valve tower and multiple valve tower [2]. The valve, during its operation, withstands high voltages and high electric-fields which are the fundamental problems related to the system insulation [3]. Generally, for monitoring of the insulation and working state of the converter valve towers, the converter station installs surveillance cameras. The cameras can only observe the working state of the converter valve tower from outside. However, it cannot directly detect other working properties of the valve modules. For example, the corona discharge occurring on the surface of valve modules, overheating on cooling fans or water leakage. If these issues cannot be observed timely, a disaster of the converter valve tower would happen during its operation. The questions how to detect the working status of valve modules and prevent

The associate editor coordinating the review of this manuscript and approving it for publication was Enamul Haque.

the fatal disaster, and avoid the hazards caused by overheating of crucial parts of valve module and leakage of water pipe, has become essential for HVDC researchers to give an analytical judgment for converter valves.

In order to detect the working status of valve modules, such as the corona discharge on the surface of a metal, cooling water leakage and local overheating on the surface of the valve component and so on, we installed full-view micro-sensor detectors in each valve component layer. A detector must be small and light so it can be attached with each valve component layer. Generally, converter valves work under a high voltage condition, the continuous opening and closing of the converter valve can produce a strong electromagnetic environment [4]. These high voltages and strong electromagnetic environment are the main challenges for the installation of the full-view micro-sensor detectors. There are some questions to be answered such as how the full-view micro-sensor detector installed on the proposed locations will affect the electric field distribution and insulation status of the valve tower; how we ensure it running safely and properly. These questions are reported by literature and several HVDC project reports and still not fully answered. To answer the aforesaid questions, this article proposes a scheme to install full-view micro-sensor detectors in the valve component layers. The authors utilized the electrostatic field simulation to analyze the electric field distribution around the valve components. This research has an essential significance for the promotion of the converter valve security and monitoring of HVDC systems in the future.

Most of previous studies focused on the time-domain and frequency-domain simulation, electromagnetic noise simulation of HVDC converter valve station, and 3D electrostatic field simulation of valve tower. For example, Guo *et al.* [5] studied the voltage distribution of the valve with different frequencies. His results showed that, under low and medium frequency conditions, the impedance parameter of the electrical system is an important factor which can affect the valve voltage distribution. Yu *et al.* [6] did simulation-based research for the time-domain wideband model of ±500kV and ±800kV converter stations. His simulation results showed the electromagnetic noise level of the ±800kV converter stations are similar to the ±500kV converter stations; Wei *et al.* [7] built an electromagnetic and electromechanical hybrid model for a Jiangsu ±800kV UHVDC project, results suggest that his proposed model can accord with the actual situation and reflect the dynamic characteristics of the UHVDC system very well. Qi *et al.* [8] studied the wideband electromagnetic noise characteristics of the vital equipment of HVDC converter station. He reported that if the key equipment works under a high voltage and a large current environment, the calculating of the integrated wideband circuit model is more accurate than that of the traditional wideband model. As per the electric-field simulation literature on the HVDC converter valve, Lei [9] performed an insulation type test simulation for the ±1100kV valve tower. He proposed the optimized structure of the shield and the aluminum beam. His Simulation results showed that the chamfer radius of the shield and the aluminum beam has a great influence on the maximum electric-field distribution of valve. Furthermore, these parameters can be adjusted to make the surface electric-field of the valve component less than 3kV/mm. Jihuan *et al.* [10] studied the electric-field distribution of valve hall of converter station by ANSYS, results showed that the maximum electric-field 2.751kV/mm of valve hall occurs on the surface of the Y-Y connected tubular bush, but it is still less than 3kV/mm. Wang *et al.* [11] had an electric-field simulation for three different types of the ±800kV valve tower, his simulation results showed that the maximum electric-fields of three different valve towers are all less than 3kV/mm. There are some other studies [12]–[15] which also focused on electric field simulation, here we cannot list all. However, relevant studies on the electric-field distribution and insulation status of valve tower after installing the full-view micro-sensor detector, are not reported by literature. In this article authors mainly studies the electric-field distribution of valve component after installing the full-view micro-sensor detector. Moreover, it discussed how the authors' proposed position for the full-view micro-sensor detector affects the electric-field distribution and insulation status of the valve tower.

Until now, we still not searched any literature about monitoring converter valve by using detector, and no engineering project reports this new technology, because the converter valve inside has a complicated electric-field environment, a small component existing can influence the insulation status and destroy the EMC balance of the whole converter system. By implanting the full-view micro-sensor detector, we can observe the running state of converter valve, if the phenomenon such as water pipes leaking, corona discharge and overheating of reactor happens, the full-view micro-sensor detector can discover timely and make the workers to process hazards quickly, so that this research has an important significance for the UHVDC theory fields and UHVDC engineering fields.

II. ±800kV CONVERTER VALVE AND SIMULATION CONDITION

A. 3D MODEL OF ±800kV CONVERTER VALVE TOWER AND FULL-VIEW MICRO-SENSOR DETECTOR

In this section, the 3D model of ±800kV converter valve tower is designed for the UHVDC system consisted of Ximeng station to Taizhou station. The 3D model is designed by Xuji Group Corporation. Fig.1 shows the electrical system of this ±800kV UHVDC project [16]. Both, the high-voltage valve hall and the low-voltage valve hall, in a single-pole station, includes a 12-pulse converter which is composed of two 6-pulse converters respectively. In a single valve hall, 6 valve towers constitute a 12-pulse converter. This ±800kV UHVDC project adopts the bipolar (positive and negative) transmission lines.

The 3D model of ±800kV converter valve tower is shown in Fig.1. This valve tower consists of two valve units,

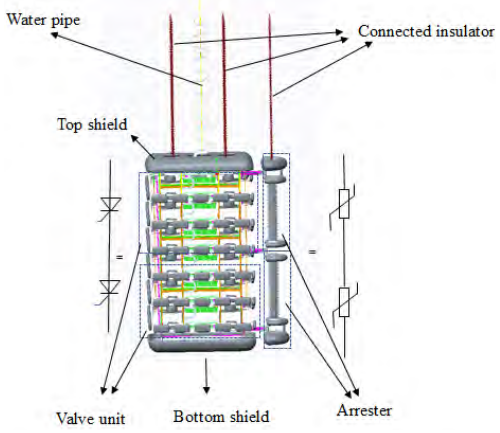

FIGURE 1. Structure model of ±800kV double-valve tower.

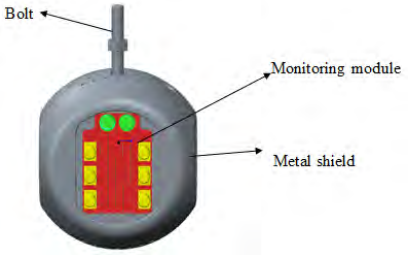

FIGURE 2. Structure of full-view micro-sensor detector.

each valve unit is composed of 6 valve components. Corresponding to the position of each valve unit, an arrester is placed. The valve tower is suspended below the valve hall by insulators, water pipes are installed from up to bottom, two adjacent valve component layers are connected by the copper busbar, each valve component layer includes 5 layer shields and 3 lateral shields, and the total number of shields is 89.

The 3D model of the full-view micro-sensor detector is shown in Fig.2. It consists of a monitoring module, a metal shield, and bolt. The monitoring module includes the PCB-board control system, the video-showing system, and the storage system. The material of the metal shield shell is aluminum and it's the purpose to prevent the monitoring module by a strong external electric-field and high-frequency magnetic field. The bolt is used to fix the full-view micro-sensor detector. The full-view micro-sensor detector is very lightweight, and the tiny in size, about 100mm×90mm×120mm. After installing the full-view micro-sensor detector on a suitable location at the valve component, the detector can detect the next layer of the valve component at 360°. The maximum imaging scope after installing the full-view micro-sensor detector is shown in Fig.3.

B. ±800kV 3D SIMPLIFIED MODEL OF VALVE COMPONENT

The full-view micro-sensor detector installed in the valve component layer can observe the working state of the next layer of the valve component. Theoretically, we can install

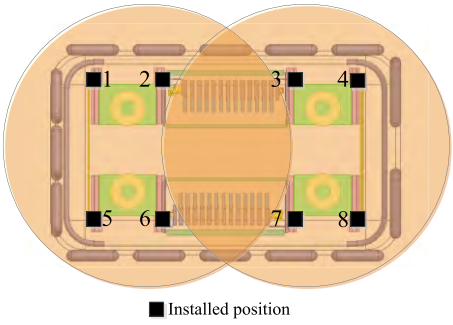

FIGURE 3. Imaging scope after installing full-view micro-sensor detector.

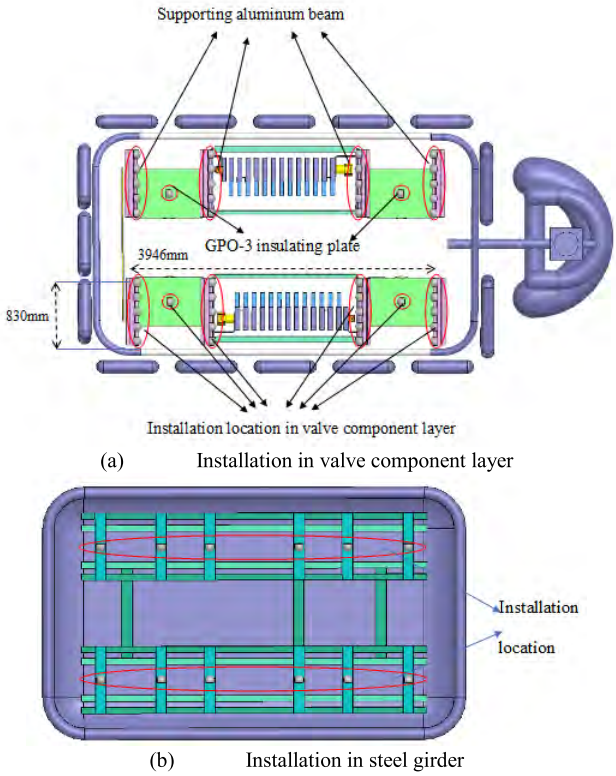

FIGURE 4. Installed locations for full-view micro-sensor detector.

4 full-view micro-sensor detectors in each valve component layer (3946mm×830mm×359mm) to cover the monitoring area of the next layer of the valve component. The proposed installed locations would be; (1) the bottom of GPO-3 insulating plate, (2) on both sides of supporting aluminum beam, (3) steel girder on the top shield, as shown in Fig.4(a). As for the top valve component, the full-view micro-sensor detector can be installed in the steel girder on the top shield. The proposed installation locations are shown in Fig.4. The material of all metal components is aluminum, whose conductivity is 3.8×10^7S/m, the dielectric constant is 1. The dielectric constant of the GPO-3 insulating plate is 4.1.

C. ELECTRIC-FIELD CALCULATION CONDITIONS

In this article, the FEM (Finite Element Method) technique is used to solve the electric-field. For the simulation,

the voltage excitation and tetrahedral mesh generation scheme was chosen. Mesh size can affect the electric-field calculation result directly. If the mesh element size is too small then it will need a lot of computational time and resources or maybe not coverage to desire solation. On the other hand, if the mesh element size is too large then it may lead to big errors in electric field results. Therefore, we propose to generate a smaller mesh element size for the critical sections and a coarse mesh element size for the non-critical sections. For example, for the shield and full-view micro-sensor detector, we set their mesh element size manually(2mm). Finally, the total number of mesh nodes is 28302493, the solving accuracy value is 0.00136, the total computational time is 12h.

As the voltage is applied to the conductor so the electric-field solving problem can be seen as the boundary-value problem of the static-electric field that can be explained by the following equation [17]:

$$I(\varphi) = \int_{\Omega} \left[\frac{1}{2} \varepsilon \nabla\varphi \cdot \nabla\varphi - \rho\varphi \right] dV + \int_{\Omega 1} \varepsilon\varphi E_n ds - \int_{\Omega 2} \varepsilon\varphi\psi ds \quad (1)$$

Here, ε is dielectric constant, ϕ is potential, V is the volume of the calculated area, ρ is volume charge density of space free body and E_{n} is an electric-field vector. The region is divided into many regions which include m number of elements and n number of nodes. If the number of elements distributed in the first boundary region and the second region are m_1 and m_2 respectively, the interpolation method can apply to solve the average potential:

$$\overline{\varphi} = \sum_{j=1}^{n} N_j \varphi_j \quad (2)$$

Here, N_{j} is the shape function of the node j and ϕ_{j} is the potential of the node j. By combine (1) with (2), and we can get the (3) [18].

$$\sum_{j=1}^{n} \left\{ \sum_{q=1}^{n} \int_{\Omega} \varepsilon \nabla N_i^q \cdot \nabla N_j^{\sigma} dV \right\} \varphi_j = \sum_{q=1}^{m} \int_{\Omega} \rho N_i^q dV - \sum_{q=1}^{m_1} \int_{\Omega 1} \varepsilon N_i^q E_n dS + \sum_{q=1}^{m_2} \int_{\Omega 2} \varepsilon N_i^q \psi dS \quad (3)$$

When $\rho = 0$, the eq.3 can be converted into the matrix:

$$S\varphi = \begin{pmatrix} S_{11} & S_{21} \\ S_{12} & S_{22} \end{pmatrix} \begin{pmatrix} \varphi \\ U \end{pmatrix} = \begin{pmatrix} F_2 \\ F_1 \end{pmatrix} \quad (4)$$

Here, S is Integral matrix, U is Potential vector of nodes distributed in the first boundary region, ϕ is the potential vector of residual nodes, F_1 is the second term of (3) and F_2 is the third term of (3). The ϕ and F_1 can be solved according to (4), vector F_1 is also equal to:

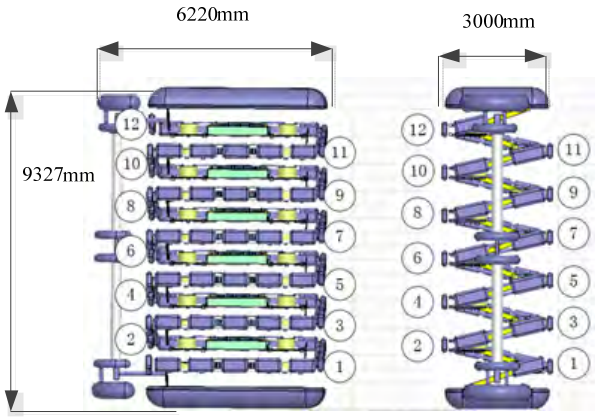

FIGURE 5. Simplified 3D model of ±800kV valve tower after installing full-view micro-sensor detector.

$$-F_1 = KE_n = \sum_{j=n_1+1}^{n} \left\{ \sum_{q=1}^{m_1} \int_{1\Omega} \varepsilon N_i^q N_j^q dS \right\} E_{nj} \quad (5)$$

Here, K is Stiffness matrix based on the first boundary region. By combing (5) with (4), the electric-field E_{n} can be solved by (6).

$$E_n = -K^{-1} \left(S_{21}\varphi + S_{22}U \right) \quad (6)$$

When the (6) is solved, the surface electric field of the conductor can be obtained.

Converter valve hall includes both, high-voltage valve hall and low-voltage valve hall. The voltage range of the low-voltage valve hall is 0-400kV, and for the high-voltage valve hall it is 400-800kV. The 800kV valve tower should withstand a higher voltage, so its insulation grade would be required higher. If the calculation result of electric-field of the 800kV valve tower meets the insulation requirement, then the insulation design of other low voltage valve tower (below 600-800kV) will be no problem. Therefore, we selected the electric-field simulation voltage range is 600-800kV and observed the electric-field distribution characteristics of valve components before and after installing the full-view micro-sensor detector. The simplified 3D model of the ±800kV valve tower is shown in Fig.5. We will not consider the 3D structure optimization of the full-view micro-sensor detector at this time, and relevant structure optimization content will be a consideration and suggested in further research.

The converter valve tower suffers an AC and DC voltage function during its operation. The potential distribution in the valve component is instantaneous. Its operating processes states can be: (1) the upper-bridge arm closing, the lower-bridge arm opening; (2) the upper bridge arm is opening, the lower bridge arm is closing; (3) the upper bridge arm and lower bridge arm both are closing. Assuming the valve tower is placed in the output of 800kV busbar and works at the second process state. We applied 820kV to the lower-bridge arm. Due to the opening of the upper-bridge arm,

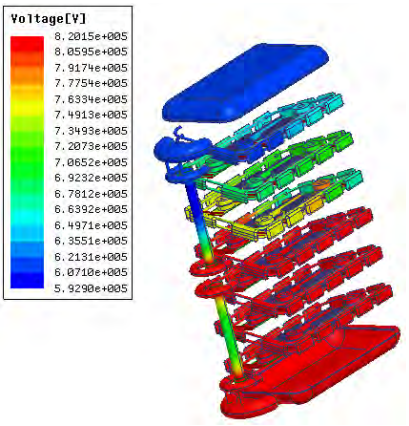

FIGURE 6. Potential distribution of valve tower.

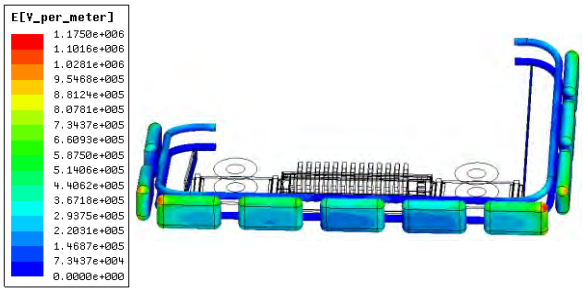

(a) Before installing

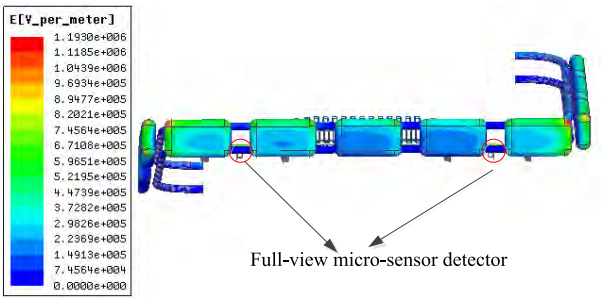

(b)After installing

FIGURE 7. Electric-field distribution of shield and water pipe near valve component 11 before and after installing full-view micro-sensor detector.

the potential of the valve module will decrease uniformly, the average decreasing voltage is 2.56kV, so the output voltage of the top shield will reach 612kV finally. Because the saturable reactor has a low resistance under a low frequency, its voltage drop is tiny, so that the saturable reactor can be seen as an equipotential body, the air conductivity is 10^{-14}S/m. The potential distribution of valve tower is shown in Fig.6.

III. ELECTRIC-FIELD CALCULATION RESULT AND ANALYSIS

As there are too many valve component layers so their simulation results are also enormous. Due to the symmetry of the valve tower, we selected the valve component layer 11 and 12 and the top shield as the research objects in this article. And the electric-field distribution, before and after installing the full-view micro-sensor detector, is observed on these the research objects.

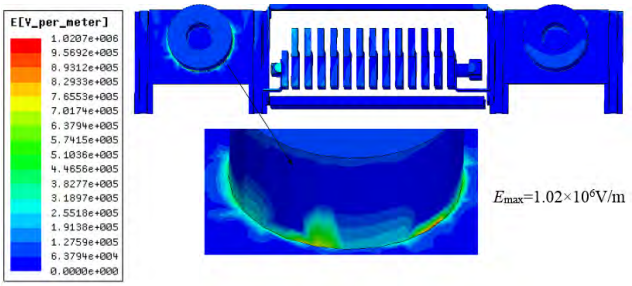

(a) Before installing

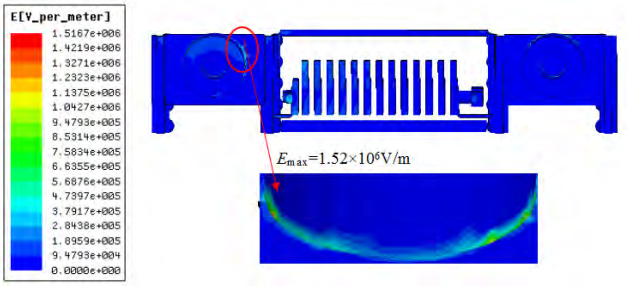

(b) After installing

FIGURE 8. Electric-field distribution of valve component 11 before and after installing full-view micro-sensor detector.

A. ELECTRIC-FIELD DISTRIBUTION OF VALVE COMPONENT BEFORE AND AFTER INSTALLING FULL-VIEW MICRO-SENSOR DETECTOR

First, we observe that how the full-view micro-sensor detector will affect the electric field distribution of shield and water pipe near the valve component layer 11 (non-direct contacted components). Simulation results show that, before installing the full-view micro-sensor detector, the maximum electric field 1.18×10^5V/m occurs at the chamfer of the corner shield. After installing the full-view micro-sensor detector, the maximum electric field value of the same position is 1.19×10^5V/m, the maximum electric field basically was not changed. It is the same as the shield and water pipe near the valve component layer 12 (results are omitted). In other words, the installation of a full-view micro-sensor detector has nearly no influence on the electric-field distribution of shield and water pipe. Therefore, we can only observe the electric field changing rule of valve component layer.

Fig.8 shows the electric field distribution of the valve component layer 11 before and after installing the full-view micro-sensor detector. Before installing the full-view micro-sensor detector (Fig.8a), the maximum electric-field 1.02×10^6V/m occurs at the contact area between the bottom of the left saturable reactor and the GPO-3 insulating plate. After installing the full-view micro-sensor detector (Fig.8b) the maximum electric field increases to 1.52×10^6V/m. This increment margin of the maximum electric field is around 0.5×10^6V/m. Therefore, the installation of a full-view micro-sensor detector influences the electric-field distribution of the valve component (direct contacted components).

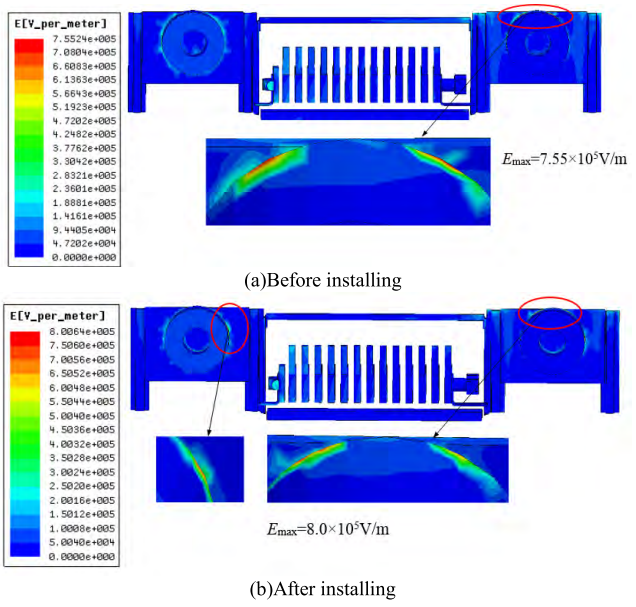

FIGURE 9. Electric-field distribution of valve component 12 before and after installing full-view micro-sensor detector.

In Fig.9 the electric-field distribution of valve component layer 12 is presented. On the layer 12, the full-view micro-sensor detector was installed and studied. The Fig.9 (a) shows the electric-field simulation result of the valve component layer 12 before and Fig.9 (b) shows after installing the full-view micro-sensor detector. Before installing the detector (Fig.9a), the maximum electric field 7.55×10^5V/m occurs at the contact area between the bottom of the right saturable reactor and the GPO-3 insulating plate, the same as the same location of the valve component layer 11. After installing the detector (Fig.9b), the maximum electric field increases to 8×10^5V/m, the increment magnitude is around 0.5×10^5V/m which is very small, can be ignored.

Next, we observe how the electric-field distribution of top shield will change before and after installing the full-view micro-sensor detector, the results are shown in Fig.10. The Fig.10 suggests that the maximum electric field of the top shield after installing the full-view micro-sensor detector was not changed radically than before. The maximum electric field was about 7.5×10^5V/m, which occurred at the outer edge of shield chamfer. Consequently, the curvature radius of the outer edge can affect the electric-field distribution. However, the inner electric field of the top shield was weakened by the outer surface and its value is small. Therefore, authors concluded that the full-view micro-sensor detector installing in the steel girder on the top shield doesn't influence the electric field distribution of the top shield and the insulation status of the top shield not has any change.

Fig.11 shows the electric field distribution of the steel girder before and after installing the full-view micro-sensor detector. Results disclosed that, before installing the full-view micro-sensor detector, the maximum electric-field on the steel girder is 1.78×10^5V/m. Whereas the maximum electric field increases to 2.49×10^5V/m after installing the full-view

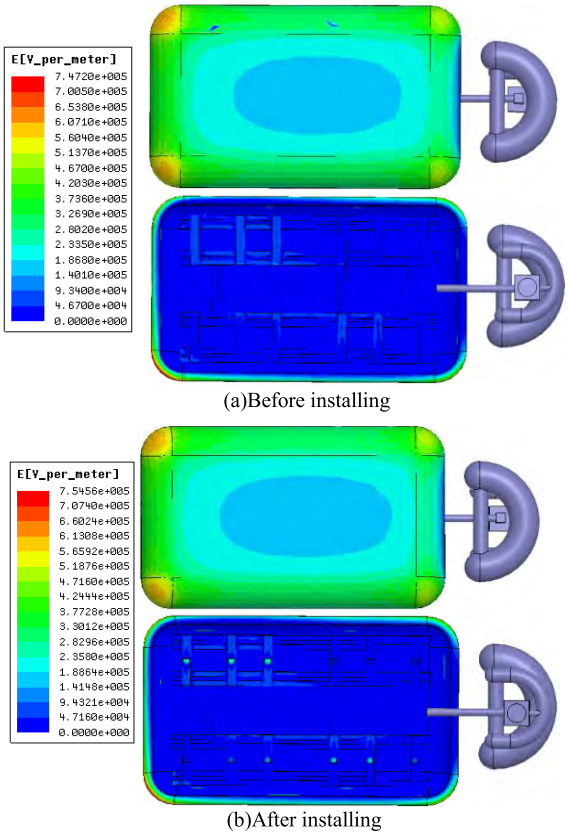

FIGURE 10. Electric-field distribution of top shield after installing full-view micro-sensor detector.

micro-sensor detector. In this case, the electric-field increases by 40%.

The Fig.11(b) shows that the maximum electric-field occurs at the surface of the full-view micro-sensor detector which is installed in the steel girder, the maximum electric field value is 4.25×10^5V/m, which is two times higher than that of the steel girder. The analysis suggested that, because the potential of the top shield is less than that of the valve module, the area between valve module and steel girder can be regarded as the ''plate-plate electrode'' area. When the full-view micro-sensor detector is installed in the steel girder, the shape of the electrode area is changed. The ''plate-plate electrode'' area could be converted into the ''sphere-plate electrode'' area. The electric-field distortion near the small radius area happened. The distortion degree of electric field increases, this leads to the increase of surface electric-field of the full-view micro-sensor detector. The electric field of the full-view micro-sensor detector installing in the steel girder is far less than 3kV/mm, so the corona discharge will not happen here.

As per the above results, the changing in the maximum electric field of valve components is summarized in Tab.1. It can be seen that after installing the full-view micro-sensor detector, the maximum electric-field of valve component 11 and 12 increases by 49% and 6% respectively. Whereas the top shield nearly has no change. The installation of the

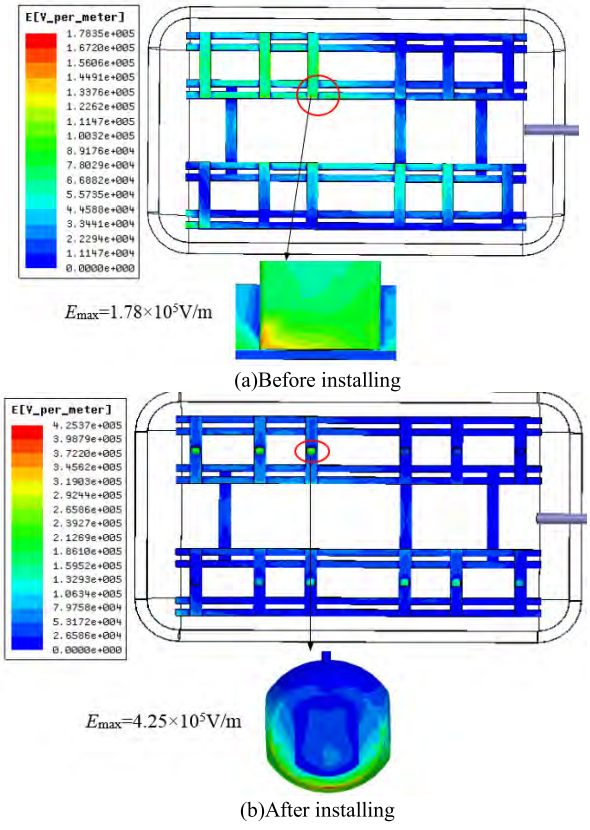

FIGURE 11. Electric-field distribution of steel girder before and after installing full-view micro-sensor detector.

TABLE 1. Maximum electric-field comparison before and after implanting full-view micro-sensor.

Electric-field（V/m）	Before installing	After installing	Amplitude
Valve component layer 11	1.02×10^6	1.52×10^6	49%↑
Valve component layer 12	7.55×10^5	8.0×10^5	6%↑
Top shield	7.47×10^5	7.54×10^5	No change
Steel girder	1.78×10^5	2.49×10^5	40%↑

full-view micro-sensor detector doesn't influence the maximum electric field distribution of the top shield, but it has a close effect on the maximum electric field distribution of the steel girder. This can be concluded that the installation of a full-view micro-sensor detector causes a rise in the electric-field of valve component, however, the maximum electric-field still meets the requirement of insulation design.

B. ELECTRIC-FIELD DISTRIBUTION OF FULL-VIEW MICRO-SENSOR DETECTOR INSTALLING AT DIFFERENT LOCATIONS

In previous subsection A, it was discussed, how the installation of a full-view micro-sensor detector affects the electric-field distribution of valve component has been studied. However, how the installed positions influence the electric field distribution of the full-view micro-sensor

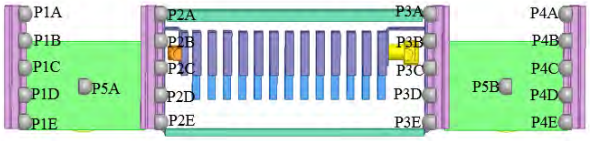

FIGURE 12. The installation ID of full-view micro-sensor detectors installed in valve component 11.

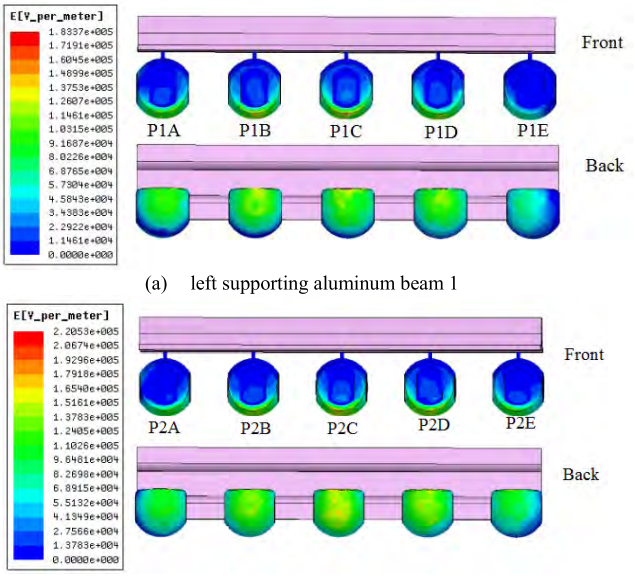

FIGURE 13. Electric-field distribution of full-view micro-sensor detectors installed in left supporting aluminum beams.

detector was not answered. As per previous subsection A, the electric-field of valve component layer 11 is higher than other studied layers. Therefore, to address this question, we select the valve component layer 11 with the full-view micro-sensor detectors as the research object and observe the electric field distribution of full-view micro-sensor detectors by installing it at different locations.

Fig.12 shows the ID number of full-view micro-sensor detectors which are installed in valve component layer 11. Full-view micro-sensor detectors are installed in left two supporting aluminum beams named; P1 and P2. The right two supporting aluminum beams named; P3 and P4. A supporting aluminum beam has 5 positions (A, B, C, D and E) to install the full-view micro-sensor detectors. Two full-view micro-sensor detectors are installed in the left and right GPO-3 insulating plate named P5A and P5B respectively.

Fig.13 shows the electric-field distribution on full-view micro-sensor detectors, which are installed in left two supporting aluminum beams.

As for the full-view micro-sensor detectors which are installed in the left supporting aluminum beam 1 (Fig.13a), the maximum electric-field 1.83×105V/m occurs at the edge of the detector's P1C but for the full-view micro-sensor detectors which are installed in the left supporting aluminum

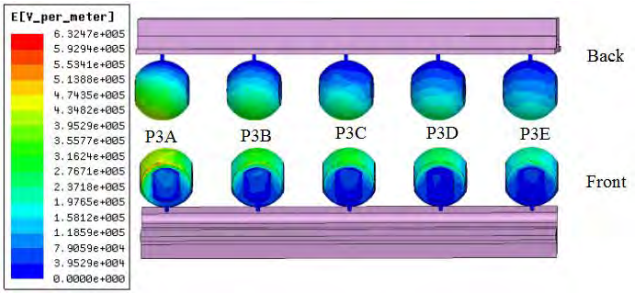

(a) right supporting aluminum beam 3

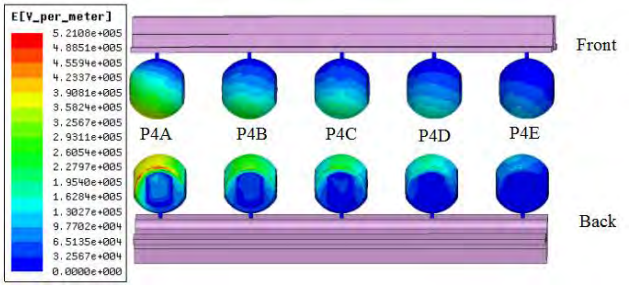

(b) right supporting aluminum beam 4

FIGURE 14. Electric-field distribution of full-view micro-sensor detectors installed in right supporting aluminum beams.

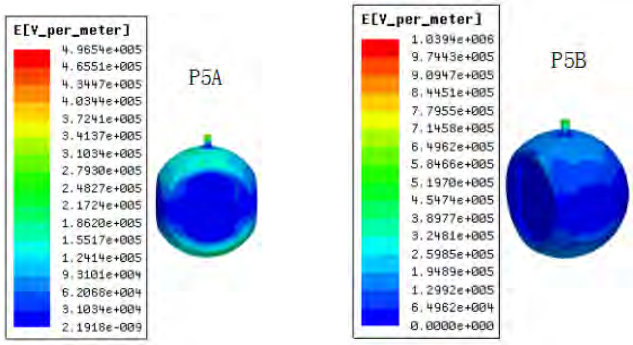

(a)Left GPO-3 (b) Right GPO-3

FIGURE 15. Electric-field distribution of full-view micro-sensor detector in GPO-3 insulating plate.

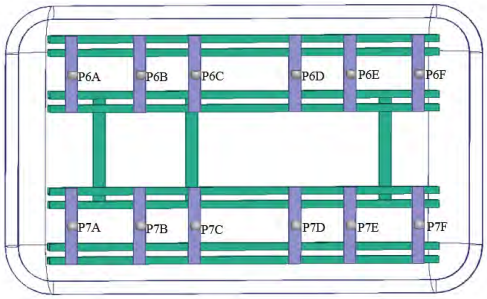

FIGURE 16. Installed location ID number of full-view micro-sensor detector in steel girder.

beam 2 and detector P2C (Fig.13b), the maximum electric field is 2.21×10^5V/m occurs at the edge of the detectors. The surface electric field of full-view micro-sensor detector installed in the left supporting aluminum beam 2, is higher than that of detectors installed in left supporting aluminum beam 1. The reason may be, the left supporting aluminum beam 2 is closed to the valve component. The electric-field lines near to this area would be distributed densely that leads to a higher electric field distribution.

The full-view micro-sensor detectors which are installed in the right supporting aluminum beam 3 and 4, their electric-field distribution is shown in Fig.14. The results show that the right supporting aluminum beam 3 is close to the valve component and the density of electric field lines is higher. That is the reason why the average surface electric-field of full-view micro-sensor detectors installed in beam 3 is higher. The maximum electric-field 6.32×10^5V/m and 5.21×10^5V/m occur at the outer edge of the monitoring module of the full-view micro-sensor detector P3A and P4A respectively which are near the water pipe.

The electric-field distribution on the full-view micro-sensor detector which is installed in the bottom of the GPO-3 insulating plate is shown in Fig.15. The results show that the surface electric field of full-view micro-sensor detectors installed in the right GPO-3 is higher than that of detectors installed in the left GPO-3. The maximum electric-field of the detector 5B is 1.04×10^6V/m. Whereas the maximum electric field 4.96×10^5V/m for the full-view micro-sensor detector is installed in the left GPO-3. It can be concluded that, when the full-view micro-sensor detector is installed in the GPO-3 insulating plate, the floating potential will be built in the metal shield and the electric-field of the full-view micro-sensor detector will be hard to control. Due to the stray capacitance effect, a large number of charges are induced at the floating position, that will cause the rise in surface electric field on the full-view micro-sensor detector. Compared to the corona electric field (3kV/mm) of air, the maximum electric-field value is still smaller.

Next, it was observed, how the electric-field will distribute on the full-view micro-sensor detectors which are installed at different locations of the steel girder. Fig.16 shows the location ID number of full-view micro-sensor detectors. Location ID P6 represents the upper steel girder, and location ID P7 represents the lower steel girder.

The electric field distribution on full-view micro-sensor detectors installed at different locations is shown in Fig.17. The results show that the maximum surface electric field on full-view micro-sensor detectors installed at P6A-P6C are in the order of magnitude of 10^5V/m but for P6D-P6F, it is in the order of magnitude of 10^4V/m. The full-view micro-sensor detectors installed on the right side have a low electric field. The maximum surface electric field on the full-view micro-sensor detectors installed at P7A-P7C is 7.6×10^4V/m to 1.5×10^5V/m and for location P7D-P7F it is about 2×10^5V/m to 3×10^5V/m. The surface electric field of full-view micro-sensor detectors is smaller. The reason, why this phenomenon happens, is that the potentials distributed in valve modules are different.

We give a maximum electric-field comparison of the full-view micro-sensor detector at different positions,

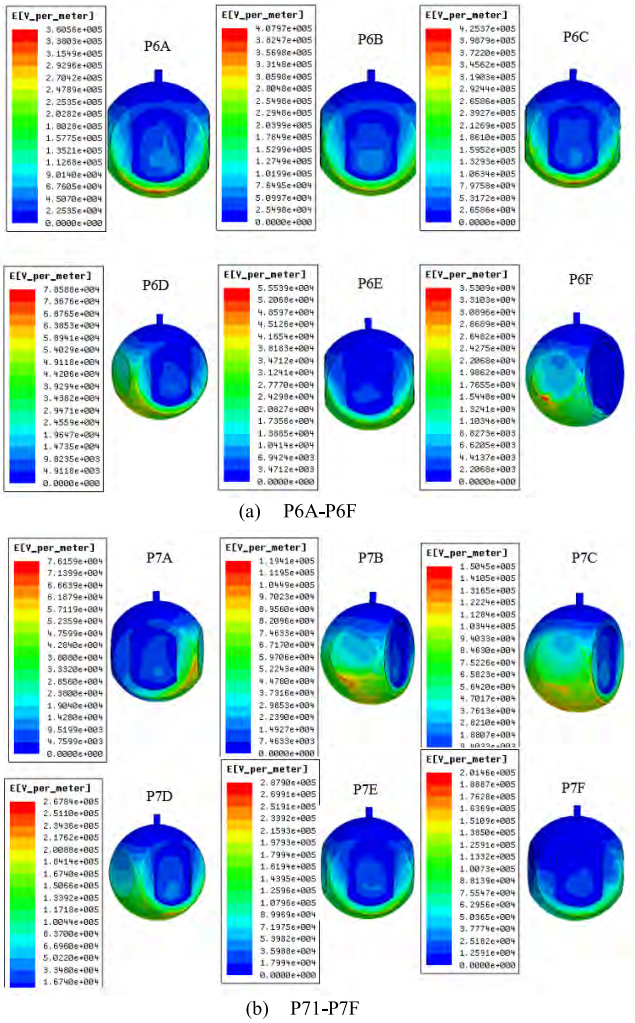

FIGURE 17. Electric-field distribution of full-view micro-sensor detectors at different locations of steel girder.

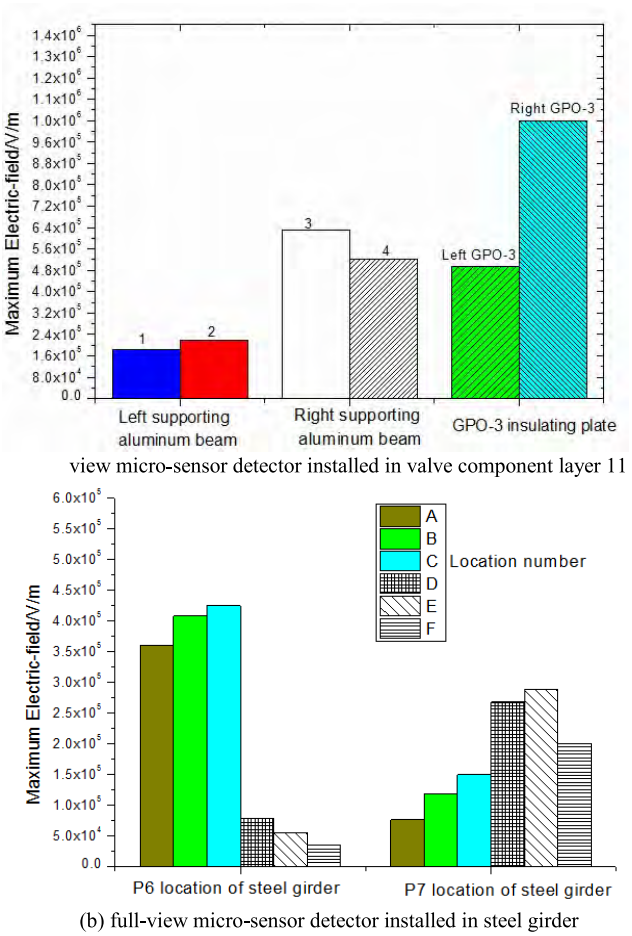

FIGURE 18. Electric-field comparison of full-view micro-sensor detector at different positions.

as shown in Fig.18. It can be seen that the electric-field of full-view micro-sensor detectors installed in the aluminum beam are smaller than that of the detector installed in the bottom of the GPO-3 insulating plate. The full-view micro-sensor detectors installed in left supporting aluminum beam have a low electric-field distribution. Whereas the maximum electric field was 1.04×10^6V/m on the full-view micro-sensor detector at the location of right GPO-3, but it is still less than 3kV/mm. Consider the floating potential that cannot be controlled easily, the full-view micro-sensor detector should be installed in supporting aluminum beams. Fig.18(b) shows that the full-view micro-sensor detector installed in P6C location of the steel girder has a maximum electric field 4.25×10^5V/m. This value is far less than 3kV/mm. Therefore, as for the steel girder, possible installation location for the full-view micro-sensor detectors, we must consider one specific implantation scheme combined with the monitoring scope of the full-view micro-sensor detector.

At present, there is still no standard for the maximum electric-field controlling of the valve component. According to the previous engineering experience, we usually consider the maximum electric-field of the valve component as 2×10^6V/m. Simulation results show that the contact area between the GPO-3 insulating plate and the saturable reactor will have a maximum electric-field 1.52×10^6V/m. The literature [20] advises that the maximum electric-field should be controlled below 1.5×10^6V/m to keep a large safety margin, so our results meet this requirement well.

IV. EXPERIMENT

A. INSULATION TYPE TEST

It is difficult to measure the electric field distribution of the full-view micro-sensor detector directly. We can do the 15s AC and 60s DC withstanding voltage insulation test for the valve tower. If the valve tower after installing the full-view micro-sensor detector doesn't have a phenomenon of corona discharge then it can verify the surface electric field of the metal component is less than 3kV/mm. The test results show that no matter either before installing the detector or after installing the detector, the corona discharge doesn't occur. This confirmed that our simulation results are correct.

In order to know whether the full-view micro-sensor detector can withstand a high impulse voltage and work properly and regularly, first, an insulation type test was

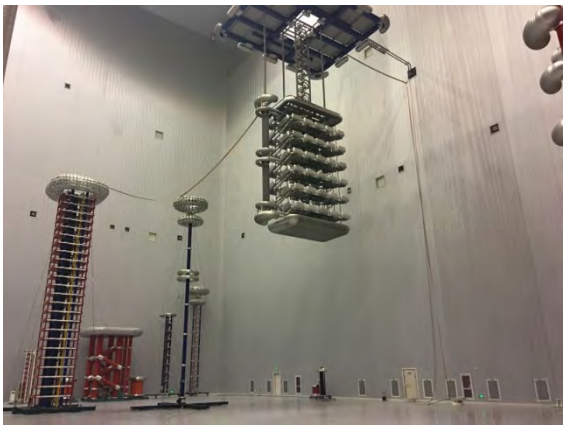

FIGURE 19. Insulation type test.

TABLE 2. LI test.

Uc(kV_p))	Polarity	Real voltage(kV_p)	T1/T2(μs)	Performance
1864.4	+	1445	1.49/44.9	Normal
		1858	1.49/45.2	Normal
		1867	1.49/45.2	Normal
		1868	1.50/45.1	Normal
		1867	1.50/45.2	Normal
	-	-1495	1.47/44.6	Normal
		-1878	1.47/44.7	Normal
		-1877	1.47/44.6	Normal
		-1880	1.48/44.5	Normal
		-1878	1.47/44.6	Normal

TABLE 3. SI test.

Uc(kV_p))	Polarity	Real voltage(kV_p)	T1/T2(μs)	Performance
1669	+	1350	244/2650	Normal
		1655	237/2660	Normal
		1665	242/2660	Normal
		1665	245/2660	Normal
		1664	248/2660	Normal
	-	-1351	238/2650	Normal
		-1665	240/2660	Normal
		-1665	249/2660	Normal
		-1671	249/2660	Normal
		-1671	243/2660	Normal

carried out. The full-view micro-sensor detectors were installed in valve component layer 11 and steel girder. The test was done in the UHVDC laboratory with Xuji Group Corporation. The testing laboratory is shown in Fig.19.

We did the SI (Switching impulse) and LI (Lightning impulse) test for the valve tower, test results are shown in Tab.2 and Tab.3.

Uc is the applied voltage value, which is proposed by State Grid Corporation. As for the LI and SI test, we did five tests for each polarity voltage. Test results show when the LI and SI voltage is applied to the valve tower, the valve component and full-view micro-sensor detector behave well and no partial flashover happens.

B. RUNNING TYPE TEST

The Fig.20 shows the result of running type test. It can be seen that, when the full-view micro-sensor detector worked under no-load condition (Fig.20a), the output voltage of

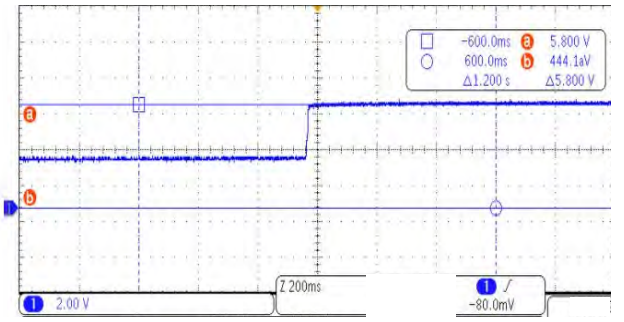

(a) No-load test

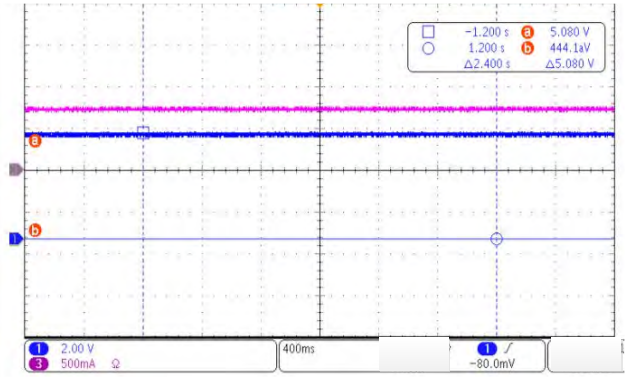

(b) Full-load test

FIGURE 20. Result of running type test.

the feature power of the full-view micro-sensor detector is 5.8V and the output waveform is steady. When the full-view micro-sensor detector worked under full-load condition (Fig.20b), the output voltage of the feature power is 5.08V. This meets the requirement that the output voltage of the feature power of the full-view micro-sensor detector cannot be smaller than 5V. In addition, we observed that the full-view micro-sensor detector could work steadily, the indicator light runs regularly, the imaging terminal can save the observed pictures.

V. CONCLUSION

The purpose of this work is to study the monitoring technology of the converter valve, and the electric field distribution of the full-view micro-sensor detector installed in the ±800kV valve component. The finding of this research can be summarized as follow:

(1) The 3D model of ±800kV converter valve tower was built. The electric field distribution of valve component 11, valve component 12 and steel girder after installing the full-view micro-sensor detector was studied. The results show that, due to the installation of full-view micro-sensor detector, the maximum electric-field of valve component 11, valve component 12 and steel girder increases by 49%, 6%, and 40% respectively. The maximum electric-field 1.52×10^6V/m occurs at the location of valve component layer 11. For the direct-contacting equipment, if the full-view micro-sensor detector was installed, it can influence the electric field

distribution but its installation almost does not affect its electric field distribution of the non-direct contacting equipment.

(2) After installing the full-view micro-sensor detector, the maximum electric field of valve components and the steel girder increases slightly than before but it is still far less than 3kV/mm. The implantation of the full-view micro-sensor detector resulted in an electric field distortion around the object. The electric-field lines around a spherical electrode were also distorted. As the distortion degree was not much large so, the maximum electric field of the valve component was not increased. The experiment also suggests that the installation idea of the full-view micro-sensor detector is feasible.

REFERENCES

[1] Y. Shu, L. Gao, and Z. Liu, "A preliminary exploration for design of ±800 kV UHVDC project with transmission capacity of 6400 MW," *Power Syst. Technol.*, vol. 30, no. 1, pp. 1–8, Jan. 2006.
[2] L. U. Zhang, A. Tiebing, and Q. I. Lei, "Electric field simulation comparative analysis of the internal valve module of ±800 kV HVDC converter valve," *Smart Grid*, vol. 3, no. 6, pp. 542–551, 2015.
[3] J. Gu, W. Zhang, X. Cui, J. Zhao, X. Li, and Q. Wang, "Research of HVDC converter valve tower radiation model," in *Proc. Asia—Pacific Microw. Conf.*, Hongkong, China, Dec. 2009, pp. 1–4.
[4] V. Vajnar and T. Nazarcik, "Service operation of UHVDC systems with emphasis on switching phenomena," in *Proc. IEEE Conf. Russian Young Researchers Elect. Electron. Eng.*, Feb. 2018, pp. 834–839.
[5] H. Guo, G. F. Tang, J. L. Wen, K. P. Zha, and X. G. Wei, "Analysis on voltage distribution performance of HVDC thyristor valves," in *Proc. IEEE Conf. Power Eng. Soc. Gen. Meeting*, San Francisco, CA, USA, Oct. 2010, pp. 1–6.
[6] Z.-Q. Yu, J.-L. He, R. Zeng, H. Rao, X.-L. Li, Q. Wang, B. Zhang, S.-M. Chen, "Simulation analysis on conducted EMD caused by valves in ± 800 kV UHVDC converter station," *IEEE Trans. Electromagn. Compat.*, vol. 51, no. 2, pp. 236–244, May 2009.
[7] P. Wei, Q. Zhou, J. K. Liu, C. G. Wang, and N. Y. Zhang, "Electromechanical-electromagnetic hybrid modelling of ±800kV Jinsu UHVDC based on real-time digital simulation device," in *Proc. 9th IET Int. Conf. AC DC Power Transmiss.*, London, U.K., 2016, pp. 28–29.
[8] L. Qi, L. Guan, Q. Shuai, J. Wen, X. Cui, X. Wei, and C. Fang, "Building and analysis of integrated wideband models for key components in HVDC converter valve systems," *IEEE Trans. Electromagn. Compat.*, vol. 56, no. 6, pp. 1697–1706, Dec. 2014.
[9] Q. Lei, W. A. Xingxing, L. I. Chao, W. A. Gaoyong, C. U. Xiang, and G. A. Chong, "Electric field simulation and optimization of ±1100 kV HVDC converter valve in insulation type test," *High Voltage Eng.*, vol. 4, no. 4, pp. 1262–1271, 2015.
[10] T. I. Jihuan, Z. H. Yuanxiang, and G. Shaowei, "Distributed parallel computation of the 3D electric field in the HVDC converter valve Hall," *High Voltage Eng.*, vol. 36, no. 5, pp. 1205–1210, 2010.
[11] J. Wang, H. Wu, Z. Deng, Z. Peng, and J. Liao, "E-field distribution analysis on three types of converter double valve in 800kV valve hall," in *Proc. 10th Int. Conf. Properties Appl. Dielectric Mater. (ICPADM)*, Jul. Jul. 2012, pp. 692–695.
[12] J. Daqian, L. Zehong , and D. Tao, "Analysis of overall electric field in high-voltage valve hall end on steady state of UHVDC system," *High Voltage Eng.*, vol. 39, no. 12, pp. 3000–3008, 2013.
[13] C. L. Liu, "Quantitative analysis of voltage distribution within ±1100kV HVDC converter valve tower under various triasient over-voltage conditions," in *Proc. Int. Conf. Lightning Protection (ICLP)*, Shanghai, China, 2014, pp. 1558–1664.
[14] H. Sun, X. Cui, and L. Du, "Electromagnetic interference prediction of ±800 kV UHVDC converter station," *IEEE Trans. Magn.*, vol. 52, no. 3, pp. 1–4, Aug. 2015.
[15] J. Cheng, Z. Peng, and J. Wang, "Electric field calculation and optimization of the UHVDC converter valve shield case," in *Proc. 10th Int. Conf. Properties Appl. Dielectric Mater. (ICPADM)*, Bangalore, India, Jul. 2012, pp. 1–4.
[16] S. Arrillaga, *High Voltage Direct Current Transmission*. London, U.K.: Peter Peregrinus Ltd., 1983.
[17] C. Xiang, "Computation of electric field intensity on the Dirichlet's boundary surface by the finite element method with constrained electric field equation on the boundary," *Chinese Soc. Elect. Eng.*, vol. 7, no. 1, pp. 51–58, 1987.
[18] X. X. Wang, X. Luo, L. Qi, and C. Li, "Calculation of electric field distribution along composite insulator and design of grading ring of HVDC converter valve," *Power Syst. Technol.*, vol. 38, no. 2, pp. 289–296, 2014.
[19] J. Wang, B. Vue, X. Deng, T. Liu, and Z. Peng, "Electric field evaluation and optimization of shielding electrodes for high voltage apparatus in ±1100 kV indoor DC yard," *IEEE Trans. Dielectr. Elect. Insul.*, vol. 25, no. 1, pp. 321–329, Feb. 2018.
[20] J. Geng, Y. Qin, F. Lv, X. Yao, and Y. Ding, "Analysis of electric field on the surface of grading and shielding fittings inside ±1100 kV ultra-high voltage converter valve hall," *High Voltage Eng.*, vol. 41, no. 11, pp. 3728–3736, 2015.

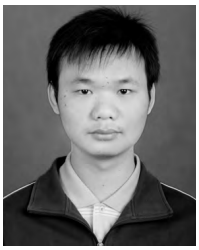

CHENYANG LIU was born in Henan, China, in 1991. He received the master's degree from Northeastern University, Shenyang, China, in 2013, and the Ph.D. degree from the State Key Laboratory of Electrical Insulation and Power Equipment, Xi'an Jiaotong University, Xi'an, China, in 2017, where he is currently a Postdoctoral Fellow. He is also an Electrical Engineer with State Grid Xuji Group Corporation. His research interests include high-voltage test technology, space radiation, electrical insulation, and UHVDC transmission technology.

SIQUAN HU, photograph and biography not available at the time of publication.

KUN HAN, photograph and biography not available at the time of publication.

QIULING HU, photograph and biography not available at the time of publication.

SHILONG GAO, photograph and biography not available at the time of publication.

WEIZHENG YAO, photograph and biography not available at the time of publication.